

# An Effective Model of the Retinoic Acid Induced HL-60 Differentiation Program

Ryan Tasseff, Holly A. Jensen, Wei Dai, Rodica P. Bunaciu<sup>†</sup>, Johanna Congleton<sup>†</sup>, Andrew Yen<sup>†</sup>, and Jeffrey D. Varner\*

Robert Frederick Smith School of Chemical and Biomolecular Engineering and <sup>†</sup>Department of Biomedical Sciences, Cornell University, Ithaca NY 14853

**Running Title:** Effective modeling of HL-60 differentiation

**To be submitted:** *Frontiers in Systems Biology*

\*Corresponding author:

Jeffrey D. Varner,

Professor, Robert Frederick Smith School of Chemical and Biomolecular Engineering,  
244 Olin Hall, Cornell University, Ithaca NY, 14853

Email: jdv27@cornell.edu

Phone: (607) 255 - 4258

Fax: (607) 255 - 9166

## **Abstract**

In this study, we present an effective model All-Trans Retinoic Acid (ATRA)-induced differentiation of HL-60 cells. The model describes a key architectural feature of ATRA-induced differentiation, positive feedback between an ATRA-inducible signalsome complex involving many proteins including Vav1, a guanine nucleotide exchange factor, and the activation of the mitogen activated protein kinase (MAPK) cascade. The model, which was developed by integrating logical rules with kinetic modeling, was significantly smaller than previous models. However, despite its simplicity, it captured key features of ATRA induced differentiation of HL-60 cells. We identified an ensemble of effective model parameters using measurements taken from ATRA-induced HL-60 cells. Using these parameters, model analysis predicted that MAPK activation was bistable as a function of ATRA exposure. Conformational experiments supported ATRA-induced bistability. These findings, combined with other literature evidence, suggest that positive feedback is central to a diversity of cell fate programs.

## **1 Introduction**

2 Understanding the architecture of differentiation programs is an important therapeutic  
3 challenge. Differentiation induction chemotherapy (DIC), using agents such as the vita-  
4 min A derivative all-trans retinoic acid (ATRA), is a promising approach for the treatment  
5 of many cancers (1–3). For example, ATRA treatment induces remission in 80–90% of  
6 promyelocytic leukemia (APL) PML-RAR $\alpha$ -positive patients (4), thereby transforming a  
7 fatal diagnosis into a manageable disease. However, remission is sometimes not durable  
8 and relapsed cases exhibit emergent ATRA resistance (5, 6). To understand the basis of  
9 this resistance, we must first understand the ATRA-induced differentiation program. To-  
10 ward this challenge, lessons learned in model systems, such as the lineage-uncommitted  
11 human myeloblastic cell line HL-60, could inform our analysis of the more complex dif-  
12 ferentiation programs occurring in patients. Patient derived HL-60 leukemia cells have  
13 been a durable experimental model since the 1970's to study differentiation (7). HL-60  
14 undergoes cell cycle arrest and either myeloid or monocytic differentiation following stim-  
15 ulation; ATRA induces G1/G0-arrest and myeloid differentiation in HL-60 cells, while 1,25-  
16 dihydroxy vitamin D3 (D3) induces arrest and monocytic differentiation. Commitment to  
17 cell cycle arrest and differentiation requires approximately 48 hr of treatment, during which  
18 HL-60 cells undergo two division cycles.

19 Sustained mitogen-activated protein kinase (MAPK) activation is a defining feature of  
20 ATRA-induced HL-60 differentiation. ATRA drives sustained MEK-dependent activation  
21 of the Raf/MEK/ERK pathway, leading to arrest and differentiation (8). MEK inhibition re-  
22 sults in the loss of ERK and Raf phosphorylation, and the failure to arrest and differentiate  
23 (9). ATRA (and its metabolites) are ligands for the hormone activated nuclear transcrip-  
24 tion factors retinoic acid receptor (RAR) and retinoid X receptor (RXR) (10). RAR/RXR  
25 activation is necessary for ATRA-induced Raf phosphorylation (9), and the formation of  
26 an ATRA-inducible signalsome complex at the membrane which drives MAPK activation

27 through a yet to be identified kinase activity. While the makeup of the signalsome com-  
28 plex is not yet known, we do know that it is composed of Src family kinases Fgr and Lyn,  
29 PI3K, c-Cbl, Slp76, and KSR, as well as IRF-1 transcription factors (11–15). Signalsome  
30 formation and activity is driven by ATRA-induced expression of CD38 and the putative  
31 heterotrimeric Gq protein-coupled receptor BLR1 (16, 17). BLR1, identified as an early  
32 ATRA (or D3)-inducible gene using differential display (18), is necessary for MAPK ac-  
33 tivation and differentiation (17), and is also involved with signalsome activity. Studies  
34 of the BLR1 promoter identified a 5' 17bp GT box approximately 1 kb upstream of the  
35 transcriptional start that conferred ATRA responsiveness (17). Members of the BLR1  
36 transcriptional activator complex, e.g. NFATc3 and CREB, are phosphorylated by ERK,  
37 JNK or p38 MAPK family members suggesting positive feedback between the signal-  
38 some and MAPK activation (19). BLR1 overexpression enhanced Raf phosphorylation  
39 and accelerated terminal differentiation, while Raf inhibition reduced BLR1 expression  
40 and differentiation (20). BLR1 knock-out cells failed to activate Raf or differentiate in  
41 the presence of ATRA (20). Interestingly, both the knockdown or inhibition of Raf, also  
42 reduced BLR1 expression and functional differentiation (20). Thus, the expression of  
43 signalsome components e.g., BLR1 was Raf dependent, while Raf activation depended  
44 upon the siganlsome. A recent computational study of ATRA-induced differentiation in  
45 HL-60 cells suggested that the BLR1-MAPK positive feedback circuit was sufficient to ex-  
46 plain ATRA-induced sustained MAPK activation, and the expression of a limited number  
47 of functional differentiation markers (21). Model analysis also suggested that Raf was the  
48 most distinct of the MAPK proteins. However, this previous study developed and analyzed  
49 a complex model, thus leaving open the critical question of what is the minimal positive  
50 feedback circuit required to drive ATRA-induced differentiation.

51 In this study, we explored this question using a minimal mathematical model of the  
52 key architectural feature of ATRA induced differentiation of HL-60 cells, namely positive

53 feedback between an ATRA-inducible signalsome complex and MAPK activation. The  
54 ATRA responsive signalsome-MAPK circuit was then used to drive a downstream gene  
55 expression program which encoded for the expression of functional differentiation mark-  
56 ers. The effective model used a novel framework which integrated logical rules with ki-  
57 netic modeling to describe gene expression and protein regulation, while largely relying  
58 upon biophysical parameters from the literature. This formulation significantly reduced  
59 the size and complexity of the model compared to the previous study of Tasseff et al.,  
60 while increasing the breadth of the biology described (21). The effective model, despite  
61 its simplicity, captured key features of ATRA induced differentiation of HL-60 cells. Model  
62 analysis predicted the bistability of MAPK activation as a function of ATRA exposure; con-  
63 formational experiments supported ATRA-induced bistability. Model simulations were also  
64 consistent with measurements of the influence of MAPK inhibitors, and the failure of BLR1  
65 knockout cells to differentiate when exposed to ATRA. Lastly, we showed by through im-  
66 munoprecipitation studies, that the guanine nucleotide exchange factor Vav1 is potentially  
67 a new ATRA-inducible member of the siganlsome complex. Taken together, these findings  
68 when combined with other literature evidence, suggested that positive feedback architec-  
69 tures are central to differentiation programs generally, and necessary for ATRA-induced  
70 differentiation.

71 **Results**

72 We constructed an effective model of ATRA-induced HL-60 differentiation which described  
73 signaling and gene expression events following the addition of ATRA (Fig. 1). The model  
74 connectivity was developed from literature and the studies presented here (Table 1). We  
75 decomposed the ATRA program into three modules; a signal initiation module that sensed  
76 and transformed the ATRA signal into activated cRaf-pS621 and the ATRA-RXR/RAR  
77 (Trigger) signals (Fig. 1A); a signal integration module that controlled the expression of  
78 upstream transcription factors given cRaf-pS621 and activated Trigger signals (Fig. 1B);  
79 and a phenotype module which encoded the expression of functional differentiation mark-  
80 ers from the ATRA-inducible transcription factors (Fig. 1C). Each component of these  
81 modules was described by a mRNA and protein balance equation. Additionally, the sig-  
82 nal initiation module also described the abundance of activated species e.g., Trigger and  
83 cRaf-pS621 whose values were derived from unactivated Trigger and cRaf protein levels.  
84 Lastly, because the population of HL-60 cells was dividing (at least before ATRA-induced  
85 cell cycle arrest), we also considered a dilution term in all balance equations. The sig-  
86 nal initiation module contained nine differential equations, while the signal integration and  
87 phenotype modules were collectively encoded by 54 differential equations. Model param-  
88 eters were taken literature (Table 2), or estimated from experimental data using heuristic  
89 optimization (see materials and methods).

90 The signal initiation module recapitulated sustained signalsome and MAPK activation  
91 following exposure to  $1\mu\text{M}$  ATRA (Fig. 2A-B). An ensemble of effective model param-  
92 eters was estimated by minimizing the difference between simulations and time-series  
93 measurements of BLR1 mRNA and cRaf-pS621 following the addition of  $1\mu\text{M}$  ATRA. We  
94 focused on the S621 phosphorylation site of cRaf since enhanced phosphorylation at  
95 this site is a defining characteristic of sustained MAPK activation in HL-60. The effective  
96 model captured both ATRA-induced BLR1 expression (Fig. 2A) and sustained phospho-

97 phosphorylation of cRaf-pS621 (Fig. 2B) in a growing population of HL-60 cells. Together, the  
98 reinforcing positive feedback between the signalsome and MAPK led to sustained activation  
99 over multiple cellular generations. However, the effective model failed to capture the  
100 decline of BLR1 message after 48 hr of ATRA exposure. This suggested that we captured  
101 the logic leading to the onset of differentiation, but failed to describe program shutdown.  
102 Next, we tested the response of the signal initiation module to different ATRA dosages.

103 The signal initiation model was bistable with respect to ATRA induction (Fig. 2C-D).  
104 Phaseplane analysis predicted two stable steady-states when ATRA was present below  
105 a critical threshold (Fig. 2C). In the lower stable state, neither the signalsome nor cRaf-  
106 pS621 were present (thus, the differentiation program was deactivated). However, at  
107 the high stable state, both the signalsome and cRaf-pS621 were present, allowing for  
108 sustained activation and differentiation. Interestingly, when ATRA was above a critical  
109 threshold, only the activated state was accessible (Fig. 2D). To test these findings, we  
110 first identified the ATRA threshold. We exposed HL-60 cells to different ATRA concen-  
111 trations for 72 hr (Fig. 2E). Morphological changes associated with differentiation were  
112 visible for ATRA  $\geq 0.25 \mu\text{M}$ , suggesting the critical ATRA threshold was near this concen-  
113 tration. Next, we conducted ATRA washout experiments to determine if activated cells  
114 remained activated in the absence of ATRA. HL-60 cells locked into an activated state  
115 remained activated following ATRA withdraw (Fig. 3). This sustained activation resulted  
116 from reinforcing feedback between the signalsome and the MAPK pathway. Thus, follow-  
117 ing activation, if we inhibited or removed elements from the signal initiation module we  
118 expected the siganlsome and MAPK signals to decay. We simulated ATRA induced acti-  
119 vation in the presence of kinase inhibitors, and without key circuit elements. Consistent  
120 with experimental results using multiple MAPK inhibitors, ATRA activation in the presence  
121 of MAPK inhibitors lowered the steady-state value of signalsome (Fig. 3A). In the pres-  
122 ence of BLR1, the signalsome and cRaf-pS621 signals were maintained following ATRA

123 withdraw (Fig. 3B, gray). On the other hand, BLR1 deletion removed the ability of the  
124 circuit to maintain a sustained MAPK response following the withdraw of ATRA (Fig. 3B,  
125 blue). Lastly, washout experiments in which cells were exposed to  $1\mu\text{M}$  ATRA for 24 hr,  
126 and then transferred to fresh media without ATRA, confirmed the persistence of the self  
127 sustaining activated state for up to 144 hr (Fig. 3C). Thus, these experiments confirmed  
128 that reinforcing positive feedback likely drives the ATRA-induced differentiation program.  
129 Next, we analyzed the ATRA-induced downstream gene expression program following  
130 signalsome and cRaf activation.

131 The signal integration and phenotype modules described ATRA-induced gene expres-  
132 sion events in wild-type HL-60 cells (Fig. 4). The signal initiation module produced two  
133 outputs, activated Trigger and cRaf-pS621 which drove the expression of ATRA-induced  
134 transcription factors, which then in turn activated the phenotypic program. In particular,  
135 Trigger, which is a surrogate for the RAR $\alpha$ /RXR transcriptional complex, regulated the ex-  
136 pression of the transcription factors CCATT/enhancer binding protein  $\alpha$  (C/EBP $\alpha$ ), PU.1,  
137 and EGR1. In turn, these transcription factors, in combination with cRaf-pS621, regulated  
138 the expression of downstream phenotypic markers such as CD38, CD11b or P47Phox.  
139 We assembled the connectivity of the signal integration and phenotypic programs driven  
140 by Trigger and cRaf-pS621 from literature (Table 1). We estimated the parameters which  
141 appeared in the control laws regulating these programs from steady-state and dynamic  
142 measurements of transcription factor and phenotypic marker expression following the ad-  
143 dition of ATRA [REFHERE]. However, the bulk of the remaining model parameters were  
144 taken from directly from literature (22) and were not estimated in this study (see mate-  
145 rials and methods). The model simulations captured the time dependent expression of  
146 CD38 and CD11b following the addition ATRA (Fig. 4A), and the steady-state for sig-  
147 nal integration and phenotypic markers (Fig. 4B). Taken together, the signal integration  
148 and phenotypic simulations were consistent with measurements, thereby validating the

149 assumed molecular connectivity.

150       The composition of the siganlsome, and the kinase ultimately responsible for medi-  
151 ating ATRA-induced Raf activation is currently unknown. To explore this question, we  
152 conducted immunoprecipitation and subsequent Western blotting to identify physical in-  
153 teractions between Raf and 19 putative interaction partners. A panel of 19 possible Raf  
154 interaction partners (kinases, GTPases, scaffolding proteins etc) was constructed based  
155 upon known signaling pathways. We did not consider the most likely binding partner, the  
156 small GTPase RAS, as previous studies have ruled it out in MAPK activation in HL-60 cells  
157 (20, 23). Total Raf was used as a bait protein for the immunoprecipitation studies. Interro-  
158 gation of the Raf interactome suggested Vav1 was involved with ATRA-induced initiation  
159 of MAPK activity (Fig. 5). Western blot analysis using total Raf and pS621 Raf specific  
160 antibodies confirmed the presence of the bait protein, total and phosphorylated forms, in  
161 the immunoprecipitate (Fig. 5A). Of the 19 proteins sampled, Vav1, Src, CK2, Akt, and  
162 14-3-3 precipitated with Raf, suggesting a direct physical interaction was possible. How-  
163 ever, only the associations between Raf and Vav1 and Raf and Src were ATRA-inducible  
164 (Fig. 5). Furthermore, the Vav1 and Src associations were correlated with pS621 Raf  
165 abundance in the precipitate. Others proteins e.g., CK2, Akt and 14-3-3, generally bound  
166 Raf regardless of phosphorylation status or ATRA treatment. The remaining 14 proteins  
167 were expressed in whole cell lysate (Fig. 5B), but were not detectable in the precipitate  
168 of Raf IP. Treatment with the Raf kinase inhibitor GW5074 following ATRA exposure re-  
169 duced the association of both Vav1 with Raf and Src with Raf (Fig. 5), although the signal  
170 intensity for Src was notably weak. However, GW5074 did not influence the association  
171 of CK2 or 14-3-3 with Raf, further demonstrating their independence from Raf phospho-  
172 rylation. Interestingly, the Raf-Akt interaction qualitatively increased following treatment  
173 with GW5074; however, it remained unaffected by treatment with ATRA. Src family ki-  
174 nases are known to be important in myeloid differentiation (24) and their role in HL-60

175 differentiation has been investigated elsewhere (11). Given the existing work and variable  
176 reproducibility in the context of the Raf immunoprecipitate, we did not investigate the role  
177 of Src further in this study. Taken together, the immunoprecipitation and GW5074 results  
178 implicated Vav1 association to be correlated with Raf activation following ATRA-treatment.  
179 Previous studies demonstrated that a Vav1-Slp76-Cbl-CD38 complex plays an important  
180 role in ATRA-induced MAPK activation and differentiation of HL-60 cells (13). Here we  
181 did not observe direct interaction of Raf with Cbl or Slp76; however, this complex could  
182 be involved upstream.

183 Next, we considered the effect of the Raf kinase inhibitor GW5074 on functional mark-  
184 ers of ATRA-induced growth arrest and differentiation. Inhibition of Raf kinase activity  
185 modulated MAPK activation and differentiation markers following ATRA exposure (Fig.  
186 5D-F). ATRA treatment alone statistically significantly increased the G1/G0 percentage  
187 over the untreated control, while GW5074 alone had a negligible effect on the cell cycle  
188 distribution (Fig. 5D). Surprisingly, the combination of GW5074 and ATRA statistically  
189 significantly increased the G1/G0 population ( $82 \pm 1\%$ ) compared with ATRA alone ( $61$   
190  $\pm 0.5\%$ ). Increased G1/G0 arrest following the combined treatment with GW5074 and  
191 ATRA was unexpected, as the combination of ATRA and the MEK inhibitor (PD98059) has  
192 been shown previously to decrease ATRA-induced growth arrest (8). However, growth ar-  
193 rest is not the sole indication of functional differentiation. Expression of the cell surface  
194 marker CD11b has also been shown to coincide with HL-60 cells myeloid differentiation  
195 (25). We measured CD11b expression, for the various treatment groups, using immuno-  
196 fluorescence flow cytometry 48 hr post-treatment. As with G1/G0 arrest, ATRA alone  
197 increased CD11b expression over the untreated control, while GW5074 further enhanced  
198 ATRA-induced CD11b expression (Fig. 5E). GW5074 alone had no statistically significant  
199 effect on CD11b expression, compared with the untreated control. Lastly, the inducible re-  
200 active oxygen species (ROS) response was used as a functional marker of differentiated

201 neutrophils (16). We measured the ROS response induced by the phorbol ester 12-O-  
202 tetradecanoylphorbol-13-acetate (TPA) using flow cytometry. Untreated cells showed no  
203 discernible TPA response, with only  $7.0 \pm 3.0\%$  ROS induction (Fig. 5F). Cells treated  
204 with ATRA had a significantly increased TPA response,  $53 \pm 7\%$  ROS induction 48 hr  
205 post-treatment. Treatment with both ATRA and GW5074 statistically significantly reduced  
206 ROS induction ( $22 \pm 0.6\%$ ) compared to ATRA alone. Interestingly, Western blot analy-  
207 sis did not detect a GW5074 effect on ATRA-induced expression of p47phox, a required  
208 upstream component of the ROS response (Fig. 5F, bottom). Thus, the inhibitory effect  
209 of GW5074 on inducible ROS might occur downstream of p47phox expression. How-  
210 ever, the ROS producing complex is MAPK dependent, therefore it is also possible that  
211 GW5074 inhibited ROS production by interfering with MAPK activation (in which case the  
212 p47Phox marker might not accurately reflect phenotypic conversion and differentiation).

213 **Discussion**

214 In this study, we presented an effective model of ATRA-inducible differentiation of HL-60  
215 cells which encoded positive feedback between the ATRA-inducible signalsome complex  
216 and the MAPK pathway. Despite its simplicity, the model captured key features of the  
217 ATRA induced differentiation such as sustained MAPK activation, and bistability with re-  
218 spect to ATRA exposure. We also reported a new ATRA-inducible component of the  
219 signalsome, Vav1. Vav1 is a guanine nucleotide exchange factor for Rho family GTPases  
220 that activate pathways leading to actin cytoskeletal rearrangements and transcriptional al-  
221 terations (26). The Vav1/Raf association correlated with Raf activity, was ATRA-inducible  
222 and decreased after treatment with GW5074. The presence of Vav1 in Raf/Grb2 com-  
223 plexes has been shown to correlate with increased Raf activity in mast cells (27). Fur-  
224 thermore, studies on Vav1 knockout mice demonstrated that the loss of Vav1 resulted  
225 in deficiencies of ERK signaling for both T-cells as well as neutrophils (28, 29). While its  
226 function in the signalsome is unclear, Vav1 has been shown to associate with a Cbl-Slp76-  
227 CD38 complex in an ATRA-dependent manner; furthermore, transfection of HL-60 cells  
228 with Cbl mutants that fail to bind CD38, yet still bind Slp76 and Vav1, prevented ATRA-  
229 induced MAPK activation (13). Thus, interaction of Cbl-Slp76-Vav1 and CD38 appears to  
230 be required for transmission of the ATRA signal by the signalsome.

231 We conducted immunoprecipitation studies and identified a limited number of ATRA-  
232 dependent and -independent Raf interaction partners. While we were unable to detect  
233 the association of Raf with common kinases and GTPases such as PKC, PKA, p38, Rac  
234 and Rho, we did establish potential interactions between Raf and key partners such as  
235 Vav1, Src, Akt, CK2 and 14-3-3. All of these partners are known to be associated with Raf  
236 activation or function. Src is known to bind Raf through an SH2 domain, and this associ-  
237 ation has been shown to be dependent of the serine phosphorylation of Raf (30). Thus,  
238 an ATRA inducible Src/Raf association may be a result of ATRA-induced Raf phospho-

rylation at S259 or S621. We also identified an interaction between Raf and the Ser/Thr  
kinases Akt and CK2. Akt can phosphorylate Raf at S259, as demonstrated by studies  
in a human breast cancer line (31). CK2 can also phosphorylate Raf, although the lit-  
erature has traditionally focused on S338 and not S621 or S259(32). However, neither  
of these kinase interactions were ATRA-inducible, suggesting their association with Raf  
alone was not associated with ATRA-induced Raf phosphorylation. The adapter protein  
14-3-3 was also constitutively associated with Raf. The interaction between Raf and 14-  
3-3 has been associated with both S621 and S259 phosphorylation and activity (33).  
Additionally, the association of Raf with 14-3-3 not only stabilized S621 phosphorylation,  
but also reversed the S621 phosphorylation from inhibitory to activating (34). Finally, we  
found that Vav1/Raf association correlated with Raf activity, was ATRA-inducible and de-  
creased after treatment with GW5074. The presence of Vav1 in Raf/Grb2 complexes has  
been shown to correlate with increased Raf activity in mast cells (27). Furthermore, stud-  
ies on Vav1 knockout mice demonstrated that the loss of Vav1 resulted in deficiencies of  
ERK signaling for both T-cells as well as neutrophils (28, 29). Interestingly, while an in-  
tegrin ligand-induced ROS response was blocked in Vav1 knockout neutrophils, TPA was  
able to bypass the Vav1 requirement and stimulate both ERK phosphorylation and ROS  
induction (29). In this study, the TPA-induced ROS response was dependent upon Raf  
kinase activity, and was mitigated by the addition of GW5074. It is possible that Vav1 is  
downstream of various integrin receptors but upstream of Raf in terms of inducible ROS  
responses. Vav1 has also been shown to associate with a Cbl-Slp76-CD38 complex in an  
ATRA-dependent manner; furthermore, transfection of HL-60 cells with Cbl mutants that  
fail to bind CD38, yet still bind Slp76 and Vav1, prevents ATRA-induced MAPK activation  
(13). The literature suggest a variety of possible receptor-signaling pathways, which in-  
volve Vav1, for MAPK activation; moreover, given the ATRA-inducible association Vav1  
may play a direct role in Raf activation.

265 We hypothesized that Vav1 is a member of an ATRA-inducible complex which propels  
266 sustained MAPK activation, arrest and differentiation. Initially, ATRA-induced Vav1 ex-  
267 pression drives increased association between Vav1 and Raf. This increased interaction  
268 facilitates phosphorylation and activation of Raf by pre-bound Akt and/or CK2 at S621  
269 or perhaps S259. Constitutively bound 14-3-3 may also stabilize the S621 phosphory-  
270 lation, modulate the activity and/or up-regulate autophosphorylation. Activated Raf can  
271 then drive ERK activation, which in turn closes the positive feedback loop by activating  
272 Raf transcription factors, e.g. Sp1 and/or STAT1 (35–38). We tested this working hy-  
273 pothesis using mathematical modeling. The model recapitulated both ATRA time-course  
274 data as well as the GW5074 inhibitor effects. This suggested the proposed Raf-Vav1  
275 architecture was at least consistent with the experimental studies. Further, analysis of  
276 the Raf-Vav1 model identified bistability in ppERK levels. Thus, two possible MAPK ac-  
277 tivation branches were possible for experimentally testable ATRA values. The analysis  
278 also suggested the ATRA-induced Raf-Vav1 architecture could be locked into a sustained  
279 signaling mode (high ppERK) even in the absence of a ATRA signal. This locked-in prop-  
280 erty could give rise to an ATRA-induction memory. We validated the treatment memory  
281 property predicted by the Raf-Vav1 circuit experimentally using ATRA-washout experi-  
282 ments. ERK phosphorylation levels remained high for more then 96 hr after ATRA was  
283 removed. Previous studies demonstrated that HL-60 cells possessed an inheritable mem-  
284 ory of ATRA stimulus (39). Although the active state was self-sustaining, the inactive state  
285 demonstrated considerable robustness to perturbation. For example, we found that 50x  
286 overexpression of Raf was required to reliably lock MAPK into the activated state, while  
287 small perturbations had almost no effect on ppERK levels over the entire ensemble. CD38  
288 expression correlated with the ppERK, suggesting its involvement in the signaling com-  
289 plex. Our computational and experimental results showed that positive feedback, through  
290 ERK-dependent Raf expression, could sustain MAPK signaling through many division cy-

291 cles. Such molecular mechanisms could underly aspects of cellular memory associated  
292 to consecutive ATRA treatments.

293 Several engineered, or naturally occurring systems involved in cell fate decisions incor-  
294 porate positive feedback and bistability (40). One of the most well studied cell fate circuits  
295 is the Mos mitogen-activated protein kinase cascade in *Xenopus* oocytes. This cascade  
296 is activated when oocytes are induced by the steroid hormone progesterone (41). The  
297 MEK-dependent activation of p42 MAPK stimulates the accumulation of the Mos onco-  
298 protein, which in turn activates MEK, thereby closing the feedback loop. This is similar to  
299 the differentiation circuit presented here; ATRA drives signalsome which activates MAPK,  
300 cell-cycle arrest, differentiation and signalsome. Thus, while HL-60 and *Xenopus* oocytes  
301 are vastly different biological models, they share similar cell fate decision architectures.  
302 Other unrelated cell fate decisions such as programmed cell death have also been sug-  
303 gested to be bistable (42). Still more biochemical networks important to human health,  
304 for example the human coagulation or complement cascades, also feature strong positive  
305 feedback elements (43). Thus, while positive feedback is sometimes not desirable in man-  
306 made systems, it may be at the core of a diverse variety of cell fate programs and other  
307 networks important to human health.

308 Model performance was impressive given its limited size. However, there were several  
309 issues to explore further. First, there was likely missing connectivity in the effective differ-  
310 entiation circuit. Decreasing BLR1 expression with simultaneously sustained cRaf-pS261  
311 activation was not captured by the current network architecture. This suggested that  
312 signalsome, once activated, had a long lifetime as decreased BLR1 expression did not  
313 impact cRaf-pS261 abundance. We could model this by separating signalsome formation  
314 into an inactive precursor pool that is transformed to a long-lived activated signalsome by  
315 MAPK activation. We should also explore adding additional downstream biological mod-  
316 ules to this skeleton model, for example the upregulation of reactive oxygen markers such

317 as p47Phox or cell cycle arrest components to capture the switch from an actively prolif-  
318 erating population to a population in G0-arrest. Next, the choice of max/min integration  
319 rules or the particular form of the transfer functions could also be explored. Integration  
320 rules other than max/min could be used, such as the mean or the product, assuming the  
321 range of the transfer functions is always  $f \in [0, 1]$ . Alternative integration rules might  
322 have different properties which could influence model identification or performance. For  
323 example, a mean integration rule would be differentiable, allowing derivative-based opti-  
324 mization approaches to be used. The form of the transfer function could also be explored.  
325 We choose hill-like functions because of their prominence in the systems and synthetic  
326 biology community. However, many other transfer functions are possible.

327 **Materials and Methods**

328 *Gene expression model equations.* We decomposed the ATRA-induced differentiation  
 329 program into three modules; a signal initiation module that sensed and transformed the  
 330 ATRA signal into activated cRaf-pS621 and the ATRA-RXR/RAR (activated Trigger) sig-  
 331 nals; a signal integration module that controlled the expression of upstream transcription  
 332 factors given cRaf-pS621 and activated Trigger signals; and a phenotype module which  
 333 encoded the expression of functional differentiation markers from the ATRA-inducible tran-  
 334 scription factors. The output of the signal initiation module was the input to the gene ex-  
 335 pression model. For each gene  $j = 1, 2, \dots, \mathcal{G}$ , we modeled both the mRNA ( $m_j$ ) and  
 336 protein ( $p_j$ ) abundance:

$$\frac{dm_j}{dt} = r_{T,j} - (\mu + \theta_{m,j}) m_j + \lambda_j \quad (1)$$

$$\frac{dp_j}{dt} = r_{X,j} - (\mu + \theta_{p,j}) p_j \quad (2)$$

337 The terms  $r_{T,j}$  and  $r_{X,j}$  denote the specific rates of transcription, and translation while  
 338 the terms  $\theta_{m,j}$  and  $\theta_{p,j}$  denote first-order degradation constants for mRNA and protein,  
 339 respectively. The specific transcription rate  $r_{T,j}$  was modeled as the product of a kinetic  
 340 term  $\bar{r}_{T,j}$  and a control term  $u_j$  which described how the abundance of transcription fac-  
 341 tors, or other regulators influenced the expression of gene  $j$ . The kinetic transcription  
 342 term  $\bar{r}_{T,j}$  was modeled as:

$$\bar{r}_{T,j} = V_T^{max} \left( \frac{L_{T,o}}{L_{T,j}} \right) \left( \frac{G_j}{K_T + G_j} \right) \quad (3)$$

343 where the maximum gene expression rate  $V_T^{max}$  was defined as the product of a char-  
 344 acteristic transcription rate constant ( $k_T$ ) and the abundance of RNA polymerase ( $R_1$ ),  
 345  $V_T^{max} = k_T (R_1)$ . The  $(L_{T,o}/L_{T,j})$  term denotes the ratio of transcription read lengths;  $L_{T,o}$

346 represents a characteristic gene length, while  $L_{T,j}$  denotes the length of gene  $j$ . Thus,  
 347 the ratio  $(L_{T,o}/L_{T,j})$  is a gene specific correction to the characteristic transcription rate  
 348  $V_T^{max}$ . The degradation rate constants were defined as  $\theta_{m,j}$  and  $\theta_{p,j}$  denote characteristic  
 349 degradation constants for mRNA and protein, respectively. Lastly, the  $\lambda_j$  term denotes the  
 350 constitutive rate of expression of gene  $j$ .

351 The gene expression control term  $0 \leq u_j \leq 1$  depended upon the combination of fac-  
 352 tors which influenced the expression of gene  $j$ . If the expression of gene  $j$  was influenced  
 353 by  $1, \dots, m$  factors, we modeled this relationship as  $u_j = \mathcal{I}_j(f_{1j}(\cdot), \dots, f_{mj}(\cdot))$  where  
 354  $0 \leq f_{ij}(\cdot) \leq 1$  denotes a regulatory transfer function quantifying the influence of factor  $i$   
 355 on the expression of gene  $j$ , and  $\mathcal{I}_j(\cdot)$  denotes an integration rule which combines the  
 356 individual regulatory inputs for gene  $j$  into a single control term. In this study, the integra-  
 357 tion rule governing gene expression was the weighted fraction of promoter configurations  
 358 that resulted in gene expression [REFHERE]:

$$u_j = \frac{W_{R_{1,j}} + \sum_n W_{nj} f_{nj}}{1 + W_{R_{1,j}} + \sum_d W_{dj} f_{dj}} \quad (4)$$

359 The numerator, the weighted sum (with weights  $W_{nj}$ ) of promoter configurations leading to  
 360 gene expression, was normalized by all possible promoter configurations. The likelihood  
 361 of each configuration was quantified by the transfer function  $f_{nj}$  (which we modeled using  
 362 hill like functions), while the lead term in the numerator  $W_{R_{1,j}}$  denotes the weight of con-  
 363 stitutive expression for gene  $j$ . Given this formulation, the rate of constitutive expression  
 364 was then given by:

$$\lambda_j = \bar{r}_{T,j} \left( \frac{W_{R_{1,j}}}{1 + W_{R_{1,j}}} \right) \quad (5)$$

365 If a gene expression process had no modifying factors,  $u_j = 1$ . Lastly, the specific trans-

<sup>366</sup> lation rate was modeled as:

$$r_{X,j} = V_X^{max} \left( \frac{L_{X,o}}{L_{X,j}} \right) \left( \frac{m_j}{K_X + m_j} \right) \quad (6)$$

<sup>367</sup> where  $V_X^{max}$  denotes a characteristic maximum translation rate estimated from literature,  
<sup>368</sup> and  $K_X$  denotes a translation saturation constant. The characteristic maximum translation  
<sup>369</sup> rate was defined as the product of a characteristic translation rate constant ( $k_X$ ) and  
<sup>370</sup> the Ribosome abundance ( $R_2$ ),  $V_X^{max} = k_X (R_2)$ . As was the case for transcription, we  
<sup>371</sup> corrected the characteristic translation rate by the ratio of the length of a characteristic  
<sup>372</sup> transcription normalized by the length of transcript  $j$ .

<sup>373</sup> *Effective cell cycle arrest model.* We formulated an effective model of the fraction of cells  
<sup>374</sup> undergoing ATRA-induced cell cycle arrest,  $\mathcal{A}$  as:

$$\frac{d\mathcal{A}}{dt} = \epsilon_1 (\text{E2F})^{\epsilon_2} \quad (7)$$

<sup>375</sup> where  $\epsilon_i$  were unknown parameters, and E2F denotes the abundance of the E2F tran-  
<sup>376</sup> scription factor. The parameters  $\epsilon_1$  and  $\epsilon_2$  were estimated from experimental cell cycle  
<sup>377</sup> distribution measurements, by discretizing and log transforming Eq. (7):

$$\log \epsilon_1 + \epsilon_2 \log (\text{E2F}_1) = \log \dot{\mathcal{A}}_{21} \quad (8)$$

$$\log \epsilon_1 + \epsilon_2 \log (\text{E2F}_2) = \log \dot{\mathcal{A}}_{32} \quad (9)$$

<sup>378</sup> where subscripts denote the experimental time point (1 = 24 hr, 2 = 48 hr, and 3 = 72 hr),  
<sup>379</sup>  $\text{E2F}_i$  denotes the E2F abundance at time point  $i$ , and  $\dot{\mathcal{A}}_{ij}$  denotes the time derivative of  
<sup>380</sup> the fraction of arrested cells estimated between time point  $i$  and  $j$  (estimated from data).  
<sup>381</sup> We calculated candidate values for  $\epsilon_j$  by solving the log-transformed system of equations  
<sup>382</sup> for 10 biological replicates.

383 *Signaling model equations.* The signal initiation, and integration modules required the  
 384 level of cRaf-pS621 and ATRA-RXR/RAR (activated Trigger) as inputs. However, our  
 385 base model described only the abundance of inactive proteins e.g., cRaf or RXR/RAR  
 386 but not the activated forms. To address this issue, we estimated pseudo steady state  
 387 approximations for the abundance of cRaf-pS621 and activated Trigger. The abundance  
 388 of activated trigger ( $x_{a,1}$ ) was estimated directly from the RXR/RAR abundance ( $x_{u,1}$ ):

$$x_{a,1} \sim x_{u,1} \left( \frac{\alpha \cdot \text{ATRA}}{1 + \alpha \cdot \text{ATRA}} \right) \quad (10)$$

389 where  $\alpha$  denotes a gain parameter;  $\alpha = 0.0$  if ATRA is less than a threshold, and  $\alpha = 0.1$   
 390 if ATRA is greater than the differentiation threshold. The abundance of cRaf-pS621 was  
 391 estimated by making the pseudo steady state approximation on the cRaf-pS621 balance.  
 392 The abundance of an activated signaling species  $i$  was given by:

$$\frac{dx_i}{dt} = r_{+,i}(\mathbf{x}, \mathbf{k}) - (\mu + k_{d,i}) x_i \quad i = 1, \dots, \mathcal{M} \quad (11)$$

393 The quantity  $x_i$  denotes concentration of signaling species  $i$ , while  $\mathcal{R}$  and  $\mathcal{M}$  denote  
 394 the number of signaling reactions and signaling species in the model, respectively. The  
 395 term  $r_{+,i}(\mathbf{x}, \mathbf{k})$  denotes the rate of generation of activated species  $i$ , while  $\mu$  denotes  
 396 the specific growth rate, and  $k_{d,i}$  denotes the rate constant controlling the non-specific  
 397 degradation of  $x_i$ . We neglected deactivation reactions e.g., phosphatase activities. We  
 398 assumed that signaling processes were fast compared to gene expression; this allowed  
 399 us to approximate the signaling balance as:

$$x_i^* \simeq \frac{r_{+,i}(\mathbf{x}, \mathbf{k})}{(\mu + k_{d,i})} \quad i = 1, \dots, \mathcal{M} \quad (12)$$

400 The generation rate was written as the product of a kinetic term ( $\bar{r}_{+,i}$ ) and a control term  
 401 ( $v_i$ ). The control terms  $0 \leq v_j \leq 1$  depended upon the combination of factors which in-  
 402 fluenced rate process  $j$ . If rate  $j$  was influenced by  $1, \dots, m$  factors, we modeled this  
 403 relationship as  $v_j = \mathcal{I}_j(f_{1j}(\cdot), \dots, f_{mj}(\cdot))$  where  $0 \leq f_{ij}(\cdot) \leq 1$  denotes a regulatory  
 404 transfer function quantifying the influence of factor  $i$  on rate  $j$ . The function  $\mathcal{I}_j(\cdot)$  is an  
 405 integration rule which maps the output of regulatory transfer functions into a control vari-  
 406 able. In this study, we used  $\mathcal{I}_j \in \{\min, \max\}$  and hill transfer functions (44). If a process  
 407 had no modifying factors,  $v_j = 1$ . The kinetic rate of cRaf-pS621 generation  $\bar{r}_{+,cRaf}$  was  
 408 modeled as:

$$\bar{r}_{+,cRaf} = k_{+,cRaf} x_s \left( \frac{x_{cRaf}}{K_{+,cRaf} + x_{cRaf}} \right) \quad (13)$$

409 where  $x_s$  denotes the signalsome abundance, and  $K_{+,cRaf}$  denotes a saturation constant  
 410 governing cRaf-pS621 formation. The formation of cRaf-pS621 was regulated by only a  
 411 single factor, the abundance of MAPK inhibitor, thus  $v_{+,cRaf}$  took the form:

$$v_{+,cRaf} = \left( 1 - \frac{I}{K_D + I} \right) \quad (14)$$

412 where  $I$  denotes the abundance of the MAPK inhibitor, and  $K_D$  denotes the inhibitor  
 413 affinity.

414 *Estimation of model parameters.* We estimated parameters appearing in the mRNA and  
 415 protein balances, and the abundance of polymerases and ribosomes, from estimates of  
 416 transcription and translation rates, the half-life of a typical mRNA and protein, and typical  
 417 values for the copies per cell of RNA polymerase and ribosomes from literature (Table 2).  
 418 For the remaining parameters, e.g., the  $W_{ij}$  appearing in the control laws, or parameters  
 419 appearing in the transfer functions  $f_{dj}$ , were estimated from the gene expression and sig-  
 420 naling data sets discussed here. The saturation constants  $K_X$  and  $K_T$  were adjusted so  
 421 that gene expression and translation resulted in gene products on a biologically realistic

concentration scale. Lastly, we calculated the concentration for gene  $G_j$  by assuming, on average, that a cell had two copies of each gene at any given time. Thus, the bulk of our gene expression parameters were based directly upon literature values, and were not adjusted during model identification. The values used for the characteristic transcription/translation parameters, degradation constants and macromolecular copy number are given in the supplemental materials along with the specific formulas required to calculate all derived constants.

Signal and gene expression model parameters were estimated by minimizing the squared difference between simulations and experimental data set  $j$ :

$$E_j(\mathbf{k}) = \sum_{i=1}^{\mathcal{T}_j} \left( \hat{\mathcal{M}}_{ij} - \hat{y}_{ij}(\mathbf{k}) \right)^2 + \left( \frac{\mathcal{M}'_{ij} - \max y_{ij}}{\mathcal{M}'_{ij}} \right)^2 \quad (15)$$

The terms  $\hat{\mathcal{M}}_{ij}$  and  $\hat{y}_{ij}$  denote scaled experimental observations and simulation outputs at time  $i$  from training set  $j$ , where  $\mathcal{T}_j$  denoted the number of time points for data set  $j$ . The first term in Eqn. (15) quantified the relative simulation error. We used immunoblot intensity measurements for model training. Thus, we trained the model on the *relative* change between bands within each data set. Suppose we have the intensity of species  $x$  at time  $\{t_1, t_2, \dots, t_n\}$  in condition  $j$ . The scaled value  $0 \leq \hat{\mathcal{M}}_{ij} \leq 1$  is given by:

$$\hat{\mathcal{M}}_{ij} = \left( \mathcal{M}_{ij} - \min_i \mathcal{M}_{ij} \right) / \left( \max_i \mathcal{M}_{ij} - \min_i \mathcal{M}_{ij} \right) \quad (16)$$

where  $\hat{\mathcal{M}}_{ij} = 0$  and  $\hat{\mathcal{M}}_{ij} = 1$  describe the lowest (highest) intensity bands. A similar scaling was used for the simulation output. The second term in the objective function ensured a realistic concentration scale was estimated by the model. We set the highest intensity band to  $\mathcal{M}'_{ij} = 10$  [AU] for all simulations. We minimized the total model residual  $\sum_j E_j$  using heuristic optimization starting from a random initial parameter guess.

442 The signaling and gene expression model equations were implemented in the Julia  
443 programming language, and solved using the ODE23s routine of the ODE package (45).  
444 The model code and parameter ensemble is freely available under an MIT software li-  
445 cense and can be downloaded from <http://www.varnerlab.org>. Model parameters esti-  
446 mated directly or derived from literature, or data presented in this study are given in Table  
447 2.

448 *Cell culture and treatment* Human myeloblastic leukemia cells (HL-60 cells) were grown  
449 in a humidified atmosphere of 5% CO<sub>2</sub> at 37°C and maintained in RPMI 1640 from Gibco  
450 (Carlsbad, CA) supplemented with 5% heat inactivated fetal bovine serum from Hyclone  
451 (Logan, UT) and 1× antibiotic/antimicotic (Gibco, Carlsbad, CA). Cells were cultured in  
452 constant exponential growth (46). Experimental cultures were initiated at  $0.1 \times 10^6$  cells/mL  
453 24 hr prior to ATRA treatment; if indicated, cells were also treated with GW5074 (2 $\mu$ M) 18  
454 hr before ATRA treatment. For the cell culture washout experiments, cells were treated  
455 with ATRA for 24 hr, washed 3x with prewarmed serum supplemented culture medium  
456 to remove ATRA, and reseeded in ATRA-free media as described. Western blot analysis  
457 was performed at incremental time points after removal of ATRA.

458 *Chemicals* All-Trans Retinoic Acid (ATRA) from Sigma-Aldrich (St. Louis, MO) was dis-  
459 solved in 100% ethanol with a stock concentration of 5mM, and used at a final concen-  
460 tration of 1 $\mu$ M (unless otherwise noted). The cRaf inhibitor GW5074 from Sigma-Aldrich  
461 (St. Louis, MO) was dissolved in DMSO with a stock concentration of 10mM, and used  
462 at a final concentration of 2 $\mu$ M. HL-60 cells were treated with 2 $\mu$ M GW5074 with or with-  
463 out ATRA (1 $\mu$ M) at 0 hr. This GW5074 dosage had a negligible effect on the cell cycle  
464 distribution, compared to ATRA treatment alone.

465 *Immunoprecipitation and western blotting* Approximately  $1.2 \times 10^7$  cells were lysed using  
466 400 $\mu$ L of M-Per lysis buffer from Thermo Scientific (Waltham, MA). Lysates were cleared

467 by centrifugation at 16,950 × g in a micro-centrifuge for 20 min at 4°C. Lysates were  
468 pre-cleared using 100 $\mu$ L protein A/G Plus agarose beads from Santa Cruz Biotechnology  
469 (Santa Cruz, CA) by inverting overnight at 4°C. Beads were cleared by centrifugation and  
470 total protein concentration was determined by a BCA assay (Thermo Scientific, Waltham,  
471 MA). Immunoprecipitations were setup by bringing lysate to a concentration of 1g/L in a  
472 total volume of 300 $\mu$ L (M-Per buffer was used for dilution). The anti-Raf antibody was  
473 added at 3 $\mu$ L. A negative control with no bait protein was also used to exclude the di-  
474 rect interaction of proteins with the A/G beads. After 1 hr of inversion at 4°C, 20 $\mu$ L of  
475 agarose beads was added and samples were left to invert overnight at 4°C. Samples  
476 were then washed three times with M-Per buffer by centrifugation. Finally proteins were  
477 eluted from agarose beads using a laemmli loading buffer. Eluted proteins were resolved  
478 by SDS-PAGE and Western blotting. Total lysate samples were normalized by total protein  
479 concentration (20 $\mu$ g per sample) and resolved by SDS-PAGE and Western blotting. Sec-  
480 ondary HRP bound antibody was used for visualization. All antibodies were purchased  
481 from Cell Signaling (Boston, MA) with the exception of  $\alpha$ -p621 Raf which was purchased  
482 from Biosource/Invitrogen (Carlsbad, CA), and  $\alpha$ -CK2 from BD Biosciences (San Jose,  
483 CA).

484 *Morphology assessment* Untreated and ATRA-treated HL-60 cells were collected after  
485 72 hr and cytocentrifuged for 3 min at 700 rpm onto glass slides. Slides were air-dried  
486 and stained with Wright's stain. Slide images were captured at 40X (Leica DM LB 100T  
487 microscope, Leica Microsystems).

488 **Competing interests**

489 The authors declare that they have no competing interests.

490 **Author's contributions**

491 J.V and A.Y directed the study. R.T, H.J and J.C conducted the cell culture measure-  
492 ments. J.V and W.D developed the reduced order HL-60 models and the parameter en-  
493 semble. W.D analyzed the model ensemble, and generated figures for the manuscript.  
494 The manuscript was prepared and edited for publication by W.D, A.Y and J.V.

495 **Acknowledgements**

496 We gratefully acknowledge the suggestions from the anonymous reviewers to improve  
497 this manuscript.

498 **Funding**

499 We acknowledge the financial support to J.V. by the National Science Foundation CA-  
500 REER (CBET-0846876) for the support of R.T. and H.J. In addition, we acknowledge  
501 support to A.Y. from the National Institutes of Health (CA 30555, CA152870) and a grant  
502 from New York State Stem Cell Science. Lastly, we acknowledge the financial support to  
503 J.V. and A.Y. from the National Cancer Institute (#U54 CA143876). The content is solely  
504 the responsibility of the authors and does not necessarily represent the official views of  
505 the National Cancer Institute or the National Institutes of Health.

506 **References**

- 507 1. Bushue N, Wan YJY (2010) Retinoid pathway and cancer therapeutics. *Adv Drug  
508 Deliv Rev* 62: 1285-98.
- 509 2. Tang XH, Gudas LJ (2011) Retinoids, retinoic acid receptors, and cancer. *Annu Rev  
510 Pathol* 6: 345-64.
- 511 3. Cheung FSG, Lovicu FJ, Reichardt JKV (2012) Current progress in using vitamin d  
512 and its analogs for cancer prevention and treatment. *Expert Rev Anticancer Ther*  
513 12: 811-37.
- 514 4. Nilsson B (1984) Probable in vivo induction of differentiation by retinoic acid of  
515 promyelocytes in acute promyelocytic leukaemia. *Br J Haematol* 57: 365-71.
- 516 5. Warrell RP Jr (1993) Retinoid resistance in acute promyelocytic leukemia: new  
517 mechanisms, strategies, and implications. *Blood* 82: 1949-53.
- 518 6. Freemantle SJ, Spinella MJ, Dmitrovsky E (2003) Retinoids in cancer therapy and  
519 chemoprevention: promise meets resistance. *Oncogene* 22: 7305-15.
- 520 7. Breitman TR, Selonick SE, Collins SJ (1980) Induction of differentiation of the hu-  
521 man promyelocytic leukemia cell line (HL-60) by retinoic acid. *Proc Natl Acad Sci U  
522 S A* 77: 2936–2940.
- 523 8. Yen A, Roberson MS, Varvayanis S, Lee AT (1998) Retinoic acid induced  
524 mitogen-activated protein (MAP)/extracellular signal-regulated kinase (ERK) kinase-  
525 dependent MAP kinase activation needed to elicit HL-60 cell differentiation and  
526 growth arrest. *Cancer Res* 58: 3163–3172.
- 527 9. Hong HY, Varvayanis S, Yen A (2001) Retinoic acid causes MEK-dependent RAF  
528 phosphorylation through RARalpha plus RXR activation in HL-60 cells. *Differentia-  
529 tion* 68: 55–66.
- 530 10. Mangelsdorf DJ, Ong ES, Dyck JA, Evans RM (1990) Nuclear receptor that identifies  
531 a novel retinoic acid response pathway. *Nature* 345: 224–229.

- 532 11. Congleton J, MacDonald R, Yen A (2012) Src inhibitors, PP2 and dasatinib, increase  
533 retinoic acid-induced association of Lyn and c-Raf (S259) and enhance MAPK-  
534 dependent differentiation of myeloid leukemia cells. Leukemia 26: 1180-8.
- 535 12. Shen M, Bunaci R, Congleton J, Jensen H, Sayam L, et al. (2011) Interferon regu-  
536 latory factor-1 binds c-Cbl, enhances mitogen activated protein kinase signaling and  
537 promotes retinoic acid-induced differentiation of HL-60 human myelo-monoblastic  
538 leukemia cells. Leuk Lymphoma 52: 2372-9.
- 539 13. Shen M, Yen A (2009) c-Cbl tyrosine kinase-binding domain mutant G306E abol-  
540 ishes the interaction of c-Cbl with CD38 and fails to promote retinoic acid-induced  
541 cell differentiation and G0 arrest. J Biol Chem 284: 25664–25677.
- 542 14. Yen A, Varvayanis S, Smith J, Lamkin T (2006) Retinoic acid induces expression of  
543 SLP-76: expression with c-FMS enhances ERK activation and retinoic acid-induced  
544 differentiation/G0 arrest of HL-60 cells. Eur J Cell Biol 85: 117–132.
- 545 15. Marchisio M, Bertagnolo V, Colamussi ML, Capitani S, Neri LM (1998) Phos-  
546 phatidylinositol 3-kinase in HL-60 nuclei is bound to the nuclear matrix and increases  
547 during granulocytic differentiation. Biochem Biophys Res Commun 253: 346-51.
- 548 16. Congleton J, Jiang H, Malavasi F, Lin H, Yen A (2011) ATRA-induced HL-60 myeloid  
549 leukemia cell differentiation depends on the CD38 cytosolic tail needed for mem-  
550 brane localization, but CD38 enzymatic activity is unnecessary. Exp Cell Res 317:  
551 910–919.
- 552 17. Wang J, Yen A (2004) A novel retinoic acid-responsive element regulates retinoic  
553 acid induced BLR1 expression. Mol Cell Biol 24: 2423 - 2443.
- 554 18. Yen A (1990) HL-60 cells as a model of growth and differentiation: the significance  
555 of variant cells. Hematology Review 4: 5-46.
- 556 19. Yang T, Xiong Q, Enslen H, Davis R, Chow CW (2002) Phosphorylation of NFATc4  
557 by p38 mitogen-activated protein kinases. Mol Cell Biol 22: 3892–3904.

- 558 20. Wang J, Yen A (2008) A MAPK-positive Feedback Mechanism for BLR1 Signaling  
559 Propels Retinoic Acid-triggered Differentiation and Cell Cycle Arrest. *J Biol Chem*  
560 283: 4375–4386.
- 561 21. Tasseff R, Nayak S, Song S, Yen A, Varner J (2011) Modeling and analysis of retinoic  
562 acid induced differentiation of uncommitted precursor cells. *Integr Biol* 3: 578 - 591.
- 563 22. Milo R, Jorgensen P, Moran U, Weber G, Springer M (2010) Bionumbers—the  
564 database of key numbers in molecular and cell biology. *Nucleic Acids Res* 38: D750-  
565 3.
- 566 23. Katagiri K, Hattori S, Nakamura S, Yamamoto T, Yoshida T, et al. (1994) Activation  
567 of ras and formation of gap complex during tpa-induced monocytic differentiation of  
568 hl-60 cells. *Blood* 84: 1780–1789.
- 569 24. Miranda MB, Johnson DE (2007) Signal transduction pathways that contribute to  
570 myeloid differentiation. *Leukemia* 21: 1363–1377.
- 571 25. Hickstein DD, Back AL, Collins SJ (1989) Regulation of expression of the cd11b and  
572 cd18 subunits of the neutrophil adherence receptor during human myeloid differen-  
573 tiation. *J Biol Chem* 264: 21812–21817.
- 574 26. Hornstein I, Alcover A, Katzav S (2004) Vav proteins, masters of the world of cy-  
575 toskeleton organization. *Cell Signal* 16: 1-11.
- 576 27. Song JS, Gomez J, Stancato LF, Rivera J (1996) Association of a p95 vav-containing  
577 signaling complex with the fcepsilonlonri gamma chain in the rbl-2h3 mast cell line.  
578 evidence for a constitutive in vivo association of vav with grb2, raf-1, and erk2 in an  
579 active complex. *J Biol Chem* 271: 26962–26970.
- 580 28. Costello PS, Walters AE, Mee PJ, Turner M, Reynolds LF, et al. (1999) The rho-  
581 family gtp exchange factor vav is a critical transducer of t cell receptor signals to the  
582 calcium, erk, and nf-kappab pathways. *Proc Natl Acad Sci U S A* 96: 3035–3040.
- 583 29. Graham D, Robertson C, Bautista J, Mascarenhas F, Diacovo M, et al. (2007)

- 584 Neutrophil-mediated oxidative burst and host defense are controlled by a Vav-  
585 PLCgamma2 signaling axis in mice. *J Clin Invest* 117: 3445–3452.
- 586 30. Cleghon V, Morrison DK (1994) Raf-1 interacts with fyn and src in a non-  
587 phosphotyrosine-dependent manner. *J Biol Chem* 269: 17749–17755.
- 588 31. Zimmermann S, Moelling K (1999) Phosphorylation and regulation of raf by akt (pro-  
589 tein kinase b). *Science* 286: 1741–1744.
- 590 32. Ritt DA, Zhou M, Conrads TP, Veenstra TD, Copeland TD, et al. (2007) Ck2 is a  
591 component of the ksr1 scaffold complex that contributes to raf kinase activation.  
592 *Curr Biol* 17: 179–184.
- 593 33. Hekman M, Wiese S, Metz R, Albert S, Troppmair J, et al. (2004) Dynamic changes  
594 in c-raf phosphorylation and 14-3-3 protein binding in response to growth factor stim-  
595 ulation: differential roles of 14-3-3 protein binding sites. *J Biol Chem* 279: 14074–  
596 14086.
- 597 34. Dhillon AS, Yip YY, Grindlay GJ, Pakay JL, Dangers M, et al. (2009) The c-terminus  
598 of raf-1 acts as a 14-3-3-dependent activation switch. *Cell Signal* 21: 1645–1651.
- 599 35. Kim HS, Lim IK (2009) Phosphorylated extracellular signal-regulated protein kinases  
600 1 and 2 phosphorylate sp1 on serine 59 and regulate cellular senescence via tran-  
601 scription of p21sdi1/cip1/waf1. *J Biol Chem* 284: 15475–15486.
- 602 36. Milanini-Mongiat J, Pouys?gur J, Pag?s G (2002) Identification of two sp1 phos-  
603 phorylation sites for p42/p44 mitogen-activated protein kinases: their implication in  
604 vascular endothelial growth factor gene transcription. *J Biol Chem* 277: 20631–  
605 20639.
- 606 37. Zhang Y, Cho YY, Petersen BL, Zhu F, Dong Z (2004) Evidence of stat1 phosphory-  
607 lation modulated by mapks, mek1 and msk1. *Carcinogenesis* 25: 1165–1175.
- 608 38. Li Z, Theus MH, Wei L (2006) Role of erk 1/2 signaling in neuronal differentiation of  
609 cultured embryonic stem cells. *Dev Growth Differ* 48: 513–523.

- 610 39. Yen A, Reece SL, Albright KL (1984) Dependence of HL-60 myeloid cell differentiation  
611 on continuous and split retinoic acid exposures: precommitment memory associated  
612 with altered nuclear structure. *J Cell Physiol* 118: 277–286.
- 613 40. Ferrell J (2002) Self-perpetuating states in signal transduction: positive feedback,  
614 double-negative feedback and bistability. *Curr Opin Cell Biol* 14: 140-8.
- 615 41. Xiong W, Ferrell J (2003) A positive-feedback-based bistable 'memory module' that  
616 governs a cell fate decision. *Nature* 426: 460-5.
- 617 42. Bagci EZ, Vodovotz Y, Billiar TR, Ermentrout GB, Bahar I (2006) Bistability in apop-  
618 tosis: roles of bax, bcl-2, and mitochondrial permeability transition pores. *Biophys J*  
619 90: 1546-59.
- 620 43. Luan D, Zai M, Varner JD (2007) Computationally derived points of fragility of a  
621 human cascade are consistent with current therapeutic strategies. *PLoS Comput  
622 Biol* 3: e142.
- 623 44. Wayman JA, Sagar A, Varner JD (2015) Dynamic modeling of cell-free biochemical  
624 networks using effective kinetic models. *Processes* 3: 138.
- 625 45. Bezanson J, Edelman A, Karpinski S, Shah VB (2014) Julia: A fresh approach to  
626 numerical computing. *CoRR* abs/1411.1607.
- 627 46. Brooks SC, Kazmer S, Levin AA, Yen A (1996) Myeloid differentiation and retinoblas-  
628 toma phosphorylation changes in HL-60 cells induced by retinoic acid receptor- and  
629 retinoid X receptor-selective retinoic acid analogs. *Blood* 87: 227–237.
- 630 47. Rishi AK, Gerald TM, Shao ZM, Li XS, Baumann RG, et al. (1996) Regulation of the  
631 human retinoic acid receptor alpha gene in the estrogen receptor negative human  
632 breast carcinoma cell lines SKBR-3 and MDA-MB-435. *Cancer Res* 56: 5246-52.
- 633 48. Mueller BU, Pabst T, Fos J, Petkovic V, Fey MF, et al. (2006) ATRA resolves the dif-  
634 ferentiation block in t(15;17) acute myeloid leukemia by restoring pu.1 expression.  
635 *Blood* 107: 3330-8.

- 636 49. Friedman AD (2007) Transcriptional control of granulocyte and monocyte develop-  
637 ment. *Oncogene* 26: 6816-28.
- 638 50. Luo XM, Ross AC (2006) Retinoic acid exerts dual regulatory actions on the ex-  
639 pression and nuclear localization of interferon regulatory factor-1. *Exp Biol Med*  
640 (Maywood) 231: 619-31.
- 641 51. Sylvester I, Schöler HR (1994) Regulation of the oct-4 gene by nuclear receptors.  
642 *Nucleic Acids Res* 22: 901-11.
- 643 52. Drach J, McQueen T, Engel H, Andreeff M, Robertson KA, et al. (1994) Retinoic  
644 acid-induced expression of cd38 antigen in myeloid cells is mediated through  
645 retinoic acid receptor-alpha. *Cancer Res* 54: 1746-52.
- 646 53. Liu M, Iavarone A, Freedman LP (1996) Transcriptional activation of the human  
647 p21(waf1/cip1) gene by retinoic acid receptor. correlation with retinoid induction of  
648 u937 cell differentiation. *J Biol Chem* 271: 31723-8.
- 649 54. Bunaciu RP, Yen A (2013) 6-formylindolo (3,2-b)carbazole (ficz) enhances retinoic  
650 acid (ra)-induced differentiation of hl-60 myeloblastic leukemia cells. *Mol Cancer* 12:  
651 39.
- 652 55. Balmer JE, Blomhoff R (2002) Gene expression regulation by retinoic acid. *J Lipid*  
653 *Res* 43: 1773-808.
- 654 56. Rosen ED, Hsu CH, Wang X, Sakai S, Freeman MW, et al. (2002) C/ebpalpha in-  
655 duces adipogenesis through ppargamma: a unified pathway. *Genes Dev* 16: 22-6.
- 656 57. Varley CL, Bacon EJ, Holder JC, Southgate J (2009) Foxa1 and irf-1 intermediary  
657 transcriptional regulators of ppargamma-induced urothelial cytodifferentiation. *Cell*  
658 *Death Differ* 16: 103-14.
- 659 58. Bruemmer D, Yin F, Liu J, Berger JP, Sakai T, et al. (2003) Regulation of the growth  
660 arrest and dna damage-inducible gene 45 (gadd45) by peroxisome proliferator-  
661 activated receptor gamma in vascular smooth muscle cells. *Circ Res* 93: e38-47.

- 662 59. Delerive P, De Bosscher K, Besnard S, Vanden Berghe W, Peters JM, et al. (1999)  
663 Peroxisome proliferator-activated receptor alpha negatively regulates the vascular  
664 inflammatory gene response by negative cross-talk with transcription factors nf-  
665 kappaB and ap-1. *J Biol Chem* 274: 32048-54.
- 666 60. Altinok S, Xu M, Spiegelman BM (1997) Ppargamma induces cell cycle withdrawal:  
667 inhibition of e2f/dp dna-binding activity via down-regulation of pp2a. *Genes Dev* 11:  
668 1987-98.
- 669 61. Fei J, Cook C, Gillespie M, Yu B, Fullen K, et al. (2011) Atherogenic  $\omega$ -6 lipids mod-  
670 ulate ppar- egr-1 crosstalk in vascular cells. *PPAR Res* 2011: 753917.
- 671 62. Song EK, Lee YR, Kim YR, Yeom JH, Yoo CH, et al. (2012) Naadp mediates insulin-  
672 stimulated glucose uptake and insulin sensitization by ppar $\gamma$  in adipocytes. *Cell Rep*  
673 2: 1607-19.
- 674 63. Szanto A, Nagy L (2005) Retinoids potentiate peroxisome proliferator-activated re-  
675 ceptor gamma action in differentiation, gene expression, and lipid metabolic pro-  
676 cesses in developing myeloid cells. *Mol Pharmacol* 67: 1935-43.
- 677 64. Han S, Sidell N, Fisher PB, Roman J (2004) Up-regulation of p21 gene expres-  
678 sion by peroxisome proliferator-activated receptor gamma in human lung carcinoma  
679 cells. *Clin Cancer Res* 10: 1911-9.
- 680 65. Von Knethen A, Brüne B (2002) Activation of peroxisome proliferator-activated re-  
681 ceptor gamma by nitric oxide in monocytes/macrophages down-regulates p47phox  
682 and attenuates the respiratory burst. *J Immunol* 169: 2619-26.
- 683 66. Dispirito JR, Fang B, Wang F, Lazar MA (2013) Pruning of the adipocyte peroxisome  
684 proliferator-activated receptor  $\gamma$  cistrome by hematopoietic master regulator pu.1.  
685 *Mol Cell Biol* 33: 3354-64.
- 686 67. Chen H, Ray-Gallet D, Zhang P, Hetherington CJ, Gonzalez DA, et al. (1995) Pu.1  
687 (spi-1) autoregulates its expression in myeloid cells. *Oncogene* 11: 1549-60.

- 688 68. Steidl U, Rosenbauer F, Verhaak RGW, Gu X, Ebralidze A, et al. (2006) Essential  
689 role of jun family transcription factors in pu.1 knockdown-induced leukemic stem  
690 cells. *Nat Genet* 38: 1269-77.
- 691 69. Laslo P, Spooner CJ, Warmflash A, Lancki DW, Lee HJ, et al. (2006) Multilineage  
692 transcriptional priming and determination of alternate hematopoietic cell fates. *Cell*  
693 126: 755-66.
- 694 70. Pahl HL, Scheibe RJ, Zhang DE, Chen HM, Galson DL, et al. (1993) The proto-  
695 oncogene pu.1 regulates expression of the myeloid-specific cd11b promoter. *J Biol*  
696 *Chem* 268: 5014-20.
- 697 71. Yuki H, Ueno S, Tatetsu H, Niiro H, Iino T, et al. (2013) Pu.1 is a potent tumor  
698 suppressor in classical hodgkin lymphoma cells. *Blood* 121: 962-70.
- 699 72. Li SL, Schlegel W, Valente AJ, Clark RA (1999) Critical flanking sequences of pu.1  
700 binding sites in myeloid-specific promoters. *J Biol Chem* 274: 32453-60.
- 701 73. Dahl R, Walsh JC, Lancki D, Laslo P, Iyer SR, et al. (2003) Regulation of macrophage  
702 and neutrophil cell fates by the pu.1:c/ebpalpha ratio and granulocyte colony-  
703 stimulating factor. *Nat Immunol* 4: 1029-36.
- 704 74. Timchenko N, Wilson DR, Taylor LR, Abdelsayed S, Wilde M, et al. (1995) Autoreg-  
705 ulation of the human c/ebp alpha gene by stimulation of upstream stimulatory factor  
706 binding. *Mol Cell Biol* 15: 1192-202.
- 707 75. Lidonnici MR, Audia A, Soliera AR, Prisco M, Ferrari-Amorotti G, et al. (2010) Ex-  
708 pression of the transcriptional repressor gfi-1 is regulated by c/ebpalpha and is  
709 involved in its proliferation and colony formation-inhibitory effects in p210bcr/abl-  
710 expressing cells. *Cancer Res* 70: 7949-59.
- 711 76. D'Alo' F, Johansen LM, Nelson EA, Radomska HS, Evans EK, et al. (2003) The  
712 amino terminal and e2f interaction domains are critical for c/ebp alpha-mediated  
713 induction of granulopoietic development of hematopoietic cells. *Blood* 102: 3163-

- 714 71.
- 715 77. Pan Z, Hetherington CJ, Zhang DE (1999) Ccaat/enhancer-binding protein activates  
716 the cd14 promoter and mediates transforming growth factor beta signaling in mono-  
717 cyte development. *J Biol Chem* 274: 23242-8.
- 718 78. Harris TE, Albrecht JH, Nakanishi M, Darlington GJ (2001) Ccaat/enhancer-binding  
719 protein-alpha cooperates with p21 to inhibit cyclin-dependent kinase-2 activity and  
720 induces growth arrest independent of dna binding. *J Biol Chem* 276: 29200-9.
- 721 79. Bauvois B, Durant L, Laboureau J, Barthélémy E, Rouillard D, et al. (1999) Upreg-  
722 ulation of cd38 gene expression in leukemic b cells by interferon types i and ii. *J*  
723 *Interferon Cytokine Res* 19: 1059-66.
- 724 80. Passioura T, Dolnikov A, Shen S, Symonds G (2005) N-ras-induced growth suppres-  
725 sion of myeloid cells is mediated by irf-1. *Cancer Res* 65: 797-804.
- 726 81. Dahl R, Iyer SR, Owens KS, Cuylear DD, Simon MC (2007) The transcriptional  
727 repressor gfi-1 antagonizes pu.1 activity through protein-protein interaction. *J Biol*  
728 *Chem* 282: 6473-83.
- 729 82. Duan Z, Horwitz M (2003) Targets of the transcriptional repressor oncoprotein gfi-1.  
730 *Proc Natl Acad Sci U S A* 100: 5932-7.
- 731 83. Chen H, Zhang P, Radomska HS, Hetherington CJ, Zhang DE, et al. (1996) Octamer  
732 binding factors and their coactivator can activate the murine pu.1 (spi-1) promoter.  
733 *J Biol Chem* 271: 15743-52.
- 734 84. Behre G, Whitmarsh AJ, Coghlan MP, Hoang T, Carpenter CL, et al. (1999) c-jun  
735 is a jnk-independent coactivator of the pu.1 transcription factor. *J Biol Chem* 274:  
736 4939-46.
- 737 85. Kardassis D, Papakosta P, Pardali K, Moustakas A (1999) c-jun transactivates the  
738 promoter of the human p21(waf1/cip1) gene by acting as a superactivator of the  
739 ubiquitous transcription factor sp1. *J Biol Chem* 274: 29572-81.

- 740 86. Johnson DG, Ohtani K, Nevins JR (1994) Autoregulatory control of e2f1 expression  
741 in response to positive and negative regulators of cell cycle progression. *Genes Dev*  
742 8: 1514-25.
- 743 87. Fu M, Zhang J, Lin Y, Zhu X, Ehrengruber MU, et al. (2002) Early growth response  
744 factor-1 is a critical transcriptional mediator of peroxisome proliferator-activated  
745 receptor-gamma 1 gene expression in human aortic smooth muscle cells. *J Biol  
746 Chem* 277: 26808-14.
- 747 88. Mak KS, Funnell APW, Pearson RCM, Crossley M (2011) Pu.1 and haematopoietic  
748 cell fate: Dosage matters. *Int J Cell Biol* 2011: 808524.
- 749 89. Chen F, Wang Q, Wang X, Studzinski GP (2004) Up-regulation of egr1 by 1,25-  
750 dihydroxyvitamin d3 contributes to increased expression of p35 activator of cyclin-  
751 dependent kinase 5 and consequent onset of the terminal phase of hl60 cell differ-  
752 entiation. *Cancer Res* 64: 5425-33.
- 753 90. Suh J, Jeon YJ, Kim HM, Kang JS, Kaminski NE, et al. (2002) Aryl hydrocarbon  
754 receptor-dependent inhibition of ap-1 activity by 2,3,7,8-tetrachlorodibenzo-p-dioxin  
755 in activated b cells. *Toxicol Appl Pharmacol* 181: 116-23.
- 756 91. Shen M, Bunaciu RP, Congleton J, Jensen HA, Sayam LG, et al. (2011) Inter-  
757 feron regulatory factor-1 binds c-cbl, enhances mitogen activated protein kinase  
758 signaling and promotes retinoic acid-induced differentiation of hl-60 human myelo-  
759 monoblastic leukemia cells. *Leuk Lymphoma* 52: 2372-9.
- 760 92. Bunaciu RP, Yen A (2011) Activation of the aryl hydrocarbon receptor ahr promotes  
761 retinoic acid-induced differentiation of myeloblastic leukemia cells by restricting ex-  
762 pression of the stem cell transcription factor oct4. *Cancer Res* 71: 2371-80.
- 763 93. Jackson DA, Pombo A, Iborra F (2000) The balance sheet for transcription: an anal-  
764 ysis of nuclear rna metabolism in mammalian cells. *FASEB J* 14: 242-54.
- 765 94. Zhao ZW, Roy R, Gebhardt JCM, Suter DM, Chapman AR, et al. (2014) Spatial orga-

- 766 nization of rna polymerase ii inside a mammalian cell nucleus revealed by reflected  
767 light-sheet superresolution microscopy. Proc Natl Acad Sci U S A 111: 681-6.
- 768 95. Freitas R, Merkle R (2004) Kinematic Self-Replicating Machines. Oxford University  
769 Press.
- 770 96. Yang E, van Nimwegen E, Zavolan M, Rajewsky N, Schroeder M, et al. (2003) De-  
771 cay rates of human mrnas: correlation with functional characteristics and sequence  
772 attributes. Genome Res 13: 1863-72.
- 773 97. Doherty MK, Hammond DE, Clague MJ, Gaskell SJ, Beynon RJ (2009) Turnover  
774 of the human proteome: determination of protein intracellular stability by dynamic  
775 silac. J Proteome Res 8: 104-12.
- 776 98. Darzacq X, Shav-Tal Y, de Turris V, Brody Y, Shenoy SM, et al. (2007) In vivo dy-  
777 namics of rna polymerase ii transcription. Nat Struct Mol Biol 14: 796-806.
- 778 99. Boström K, Wettesten M, Borén J, Bondjers G, Wiklund O, et al. (1986) Pulse-chase  
779 studies of the synthesis and intracellular transport of apolipoprotein b-100 in hep g2  
780 cells. J Biol Chem 261: 13800-6.
- 781 100. Meyers R, editor (2004) Encyclopedia of Molecular Cell Biology and Molecular  
782 Medicine, Volume 1, 2nd Edition. ISBN: 978-3-527-30543-8. Wiley-Blackwell.
- 783 101. Rosenbluth MJ, Lam WA, Fletcher DA (2006) Force microscopy of nonadherent  
784 cells: a comparison of leukemia cell deformability. Biophys J 90: 2994-3003.
- 785 102. Jensen HA, Yourish HB, Bunaciu RP, Varner JD, Yen A (2015) Induced myelomono-  
786 cytic differentiation in leukemia cells is accompanied by noncanonical transcription  
787 factor expression. FEBS Open Bio 5: 789-800.

**Table 1:** Myelomonocytic transcription factor connectivity used in the signal integration and phenotype modules.

788

789

Effector	Effect	Target	Source
RAR $\alpha$	+	RAR $\alpha$	(47)
	+	PU.1	(48)
	+	C/EBP $\alpha$	(49)
	+	IRF-1	(50)
	-	Oct4	(51)
	+	CD38	(52)
	+	p21	(53)
	+	AhR	(54)
	+	EGR1	(55)
PPAR $\gamma$	+	C/EBP $\alpha$	(56)
	+	IRF-1	(57)
	+	Oct1	(58)
	-	AP-1	(59)
	-	E2F	(60)
	-	EGR1	(61)
	+	CD38	(62)
	+	CD14	(63)
	+	p21	(64)
	-	p47phox	(65)
PU.1	-	PPAR $\gamma$	(66)
	+	PU.1	(67)
	+	AP-1	(68)
	+	EGR1	(69)
	+	CD11b	(70)
	+	p21	(71)
	+	p47phox	(72)
C/EBP $\alpha$	+	PPAR $\gamma$	(56)
	+	PU.1	(73)
	+	C/EBP $\alpha$	(74)
	+	Gfi-1	(75)
	-	E2F	(76)
	+	CD14	(77)

	+	p21	(78)
IRF-1	+	CD38	(79)
	+	p21	(80)
	-	PU.1	(81)
	-	C/EBP $\alpha$	(82)
	-	E2F	(82)
	-	EGR1	(69)
	-	p21	(82)
Oct1	+	PU.1	(83)
AP-1	-	PPAR $\gamma$	(59)
	+	PU.1	(84)
	+	p21	(85)
E2F	+	E2F	(86)
EGR1	+	PPAR $\gamma$	(87)
	-	Gfi-1	(88)
	+	CD14	(89)
AhR	+	AP-1	(90)
	+	IRF-1	(91)
	-	Oct4	(92)
	-	PU.1	

**Table 2:** Characteristic model parameters estimated from literature.

Symbol	Description	Value	Units	Source	
$R_1$	RNA polymerase abundance	75,000	copies/cell	(93, 94)	
$R_2$	Ribosome abundance	$1 \times 10^6$	copies/cell	(95)	
$G_i$	Characteristic gene abundance	2	copies/cell	this study	
$K_X$	Saturation constant transcription	4,600	copies/cell	this study	
$K_T$	Saturation constant translation	100,000	copies/cell	this study	
$t_{1/2,m}$	characteristic mRNA half-life (transcription factor)	2	hr	(96)	
$t_{1/2,p}$	characteristic protein half-life	10	hr	(97)	
$\theta_{m,j}$	characteristic mRNA degradation constant	0.34	$hr^{-1}$	derived	
$\theta_{p,j}$	characteristic protein degradation constant	0.07	$hr^{-1}$	derived	
792	$t_d$	HL-60 doubling time	19.5	hr	this study
	$\mu$	growth rate	0.035	$hr^{-1}$	derived
	$k_d$	death rate	$0.10\mu$	$hr^{-1}$	derived
$e_T$	elongation rate RNA polymerase	6	nt/s	(98)	
$e_X$	elongation rate Ribosome	5	aa/s	(99)	
$L_{T,o}$	characteristic gene length	15,000	nt	(100)	
$L_{X,o}$	characteristic transcript length	5,000	nt	derived	
$k_T$	characteristic transcription rate	1.44	$hr^{-1}$	derived	
$k_X$	characteristic translation rate	3.60	$hr^{-1}$	derived	
$D$	Diameter of an HL-60 cell	12.4	$\mu m^3$	(101)	
$f_C$	cytoplasmic fraction	0.51	dimensionless	(101)	

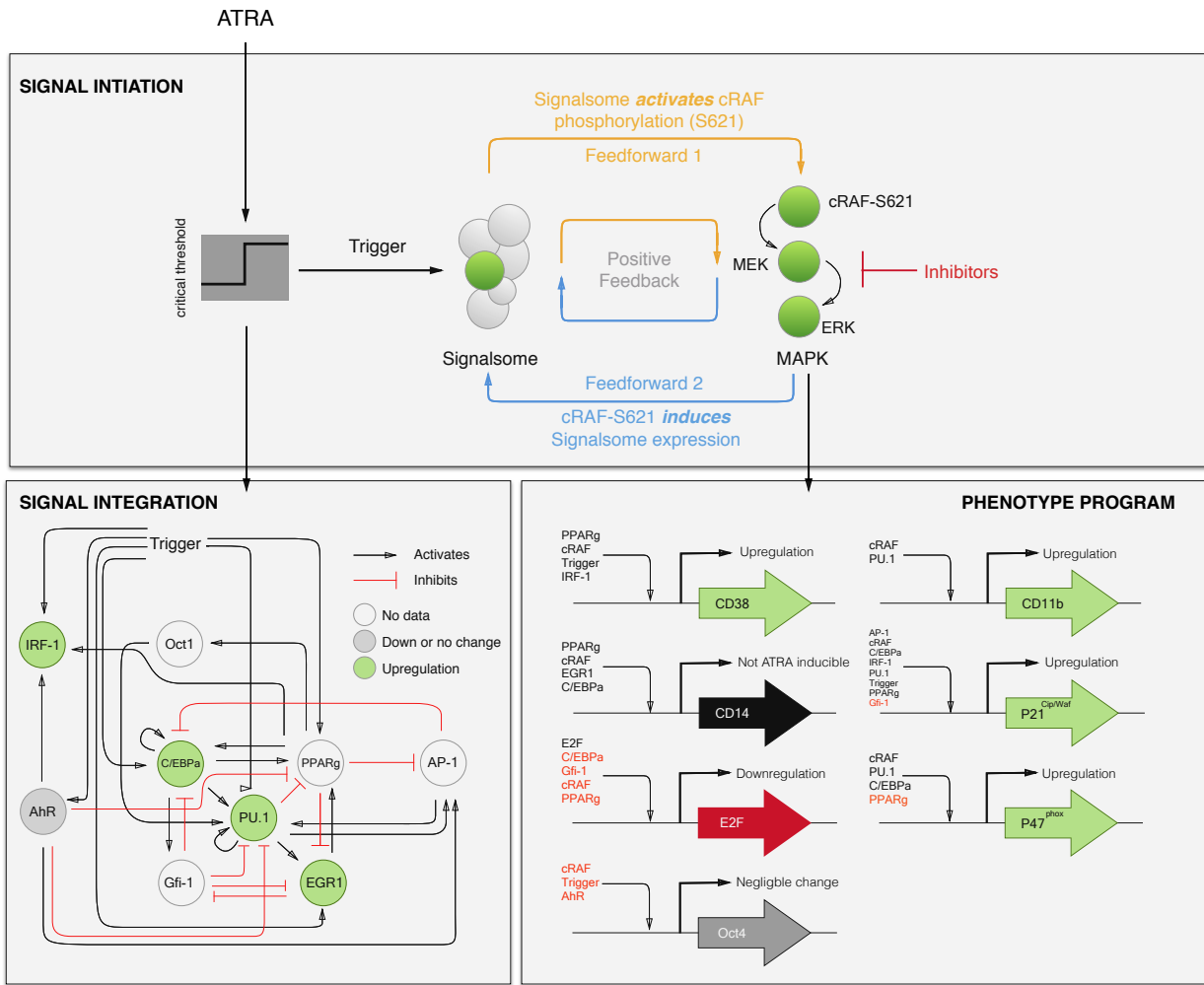


**Fig. 1:** Schematic of the effective ATRA differentiation circuit. Above a critical threshold, ATRA activates an upstream Trigger, which induces signalsome complex formation. Signalsome activates the mitogen-activated protein kinase (MAPK) cascade which in turn drives the differentiation program and signalsome formation. Both Trigger and activated cRaf-pS621 drive a phenotype gene expression program responsible for differentiation. Trigger activates the expression of a series of transcription factors which in combination with cRaf-pS621 result in phenotypic change.

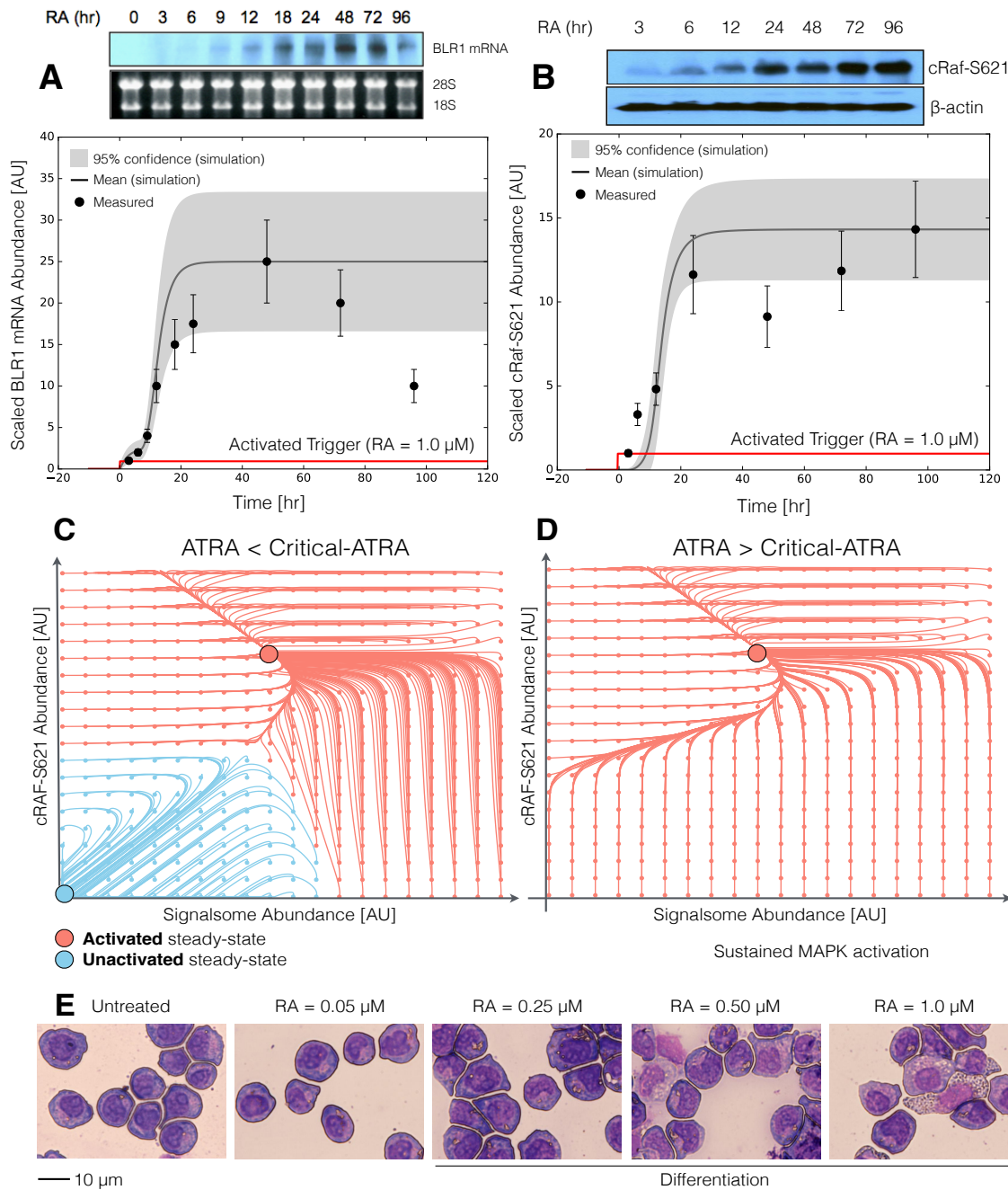


**Fig. 2:** Model analysis for ATRA-induced HL-60 differentiation. A: BLR1 mRNA versus time following exposure to  $1\mu\text{M}$  ATRA at  $t = 0$  hr. B: cRaf-pS621 versus time following exposure to  $1\mu\text{M}$  ATRA at  $t = 0$  hr. Points denote experimental measurements, solid lines denote the mean model performance. Shaded regions denote the 99% confidence interval calculated over the parameter ensemble. C: Signalsome and cRaf-pS621 nullclines for ATRA below the critical threshold. The model had two stable steady states and a single unstable state in this regime. D: Signalsome and cRaf-pS621 nullclines for ATRA above the critical threshold. In this regime the model had only a single stable steady state. E: Morphology of HL-60 as a function of ATRA concentration ( $t = 72$  hr).

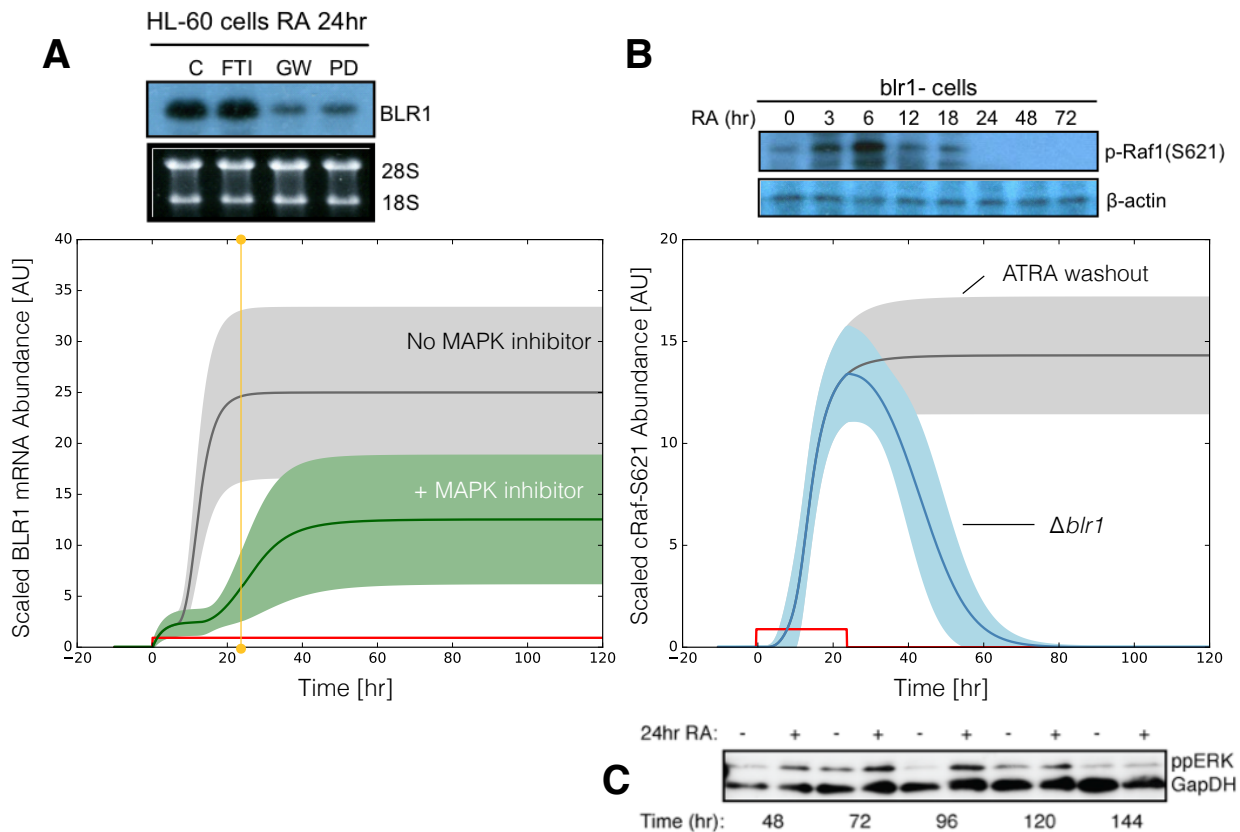


**Fig. 3:** Model simulation following exposure to  $1\mu\text{M}$  ATRA. A: BLR1 mRNA versus time with and without MAPK inhibitor. B: cRaf-pS621 versus time following pulsed exposure to  $1\mu\text{M}$  ATRA with and without BLR1. Solid lines denote the mean model performance, while shaded regions denote the 99% confidence interval calculated over the parameter ensemble. C: Western blot analysis of phosphorylated ERK1/2 in ATRA washout experiments. Experimental data in panels A and B were reproduced from Wang and Yen (20), data in panel C is reported in this study.

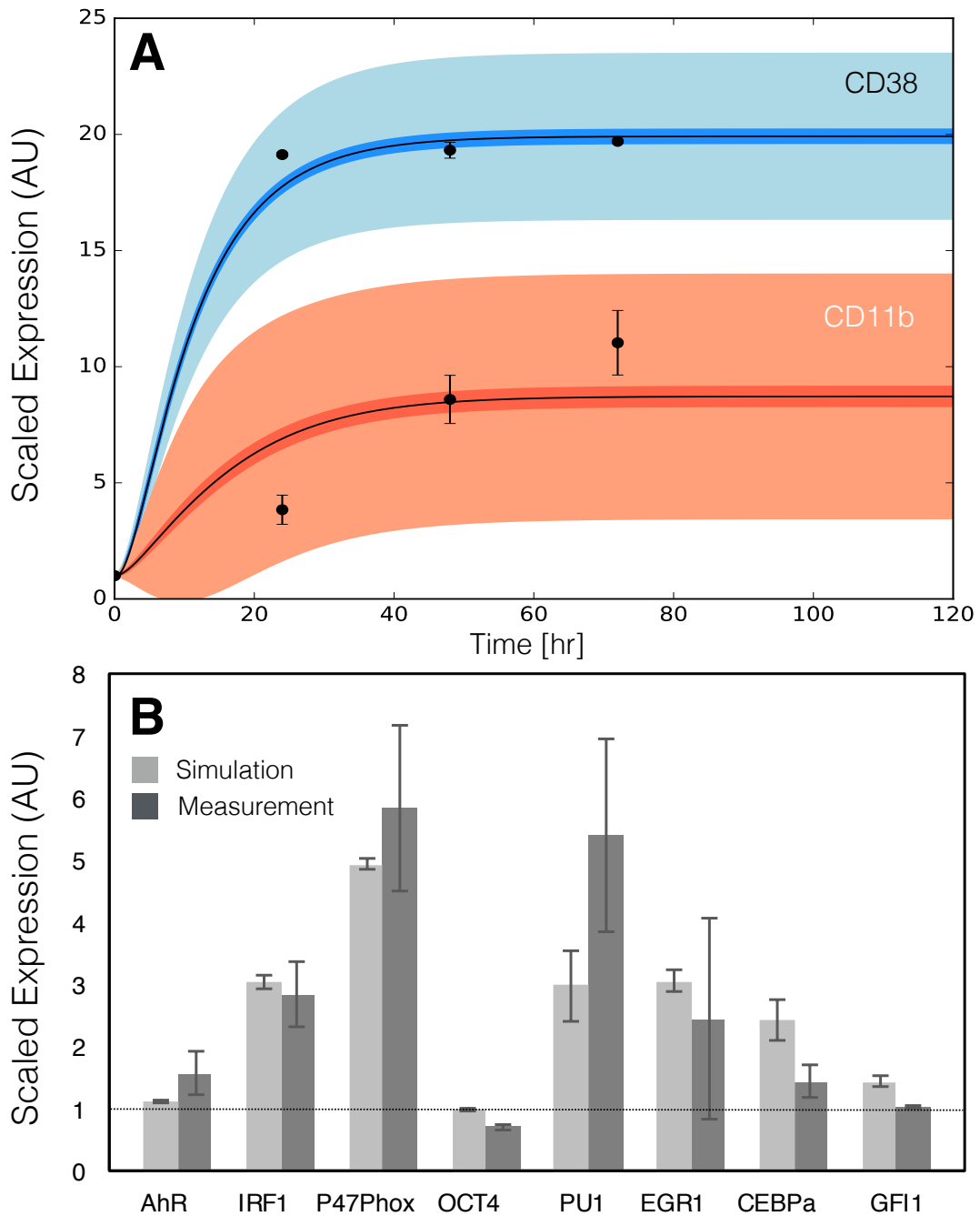


**Fig. 4:** Model simulation of the HL-60 gene expression program following exposure to  $1\mu\text{M}$  ATRA at  $t = 0$  hr. A: CD38 and CD11b expression versus time following ATRA exposure at time  $t = 0$  hr. B: Gene expression at  $t = 48$  hr following ATRA exposure. Experimental data in panels A and B were reproduced from Jensen et al. (102).

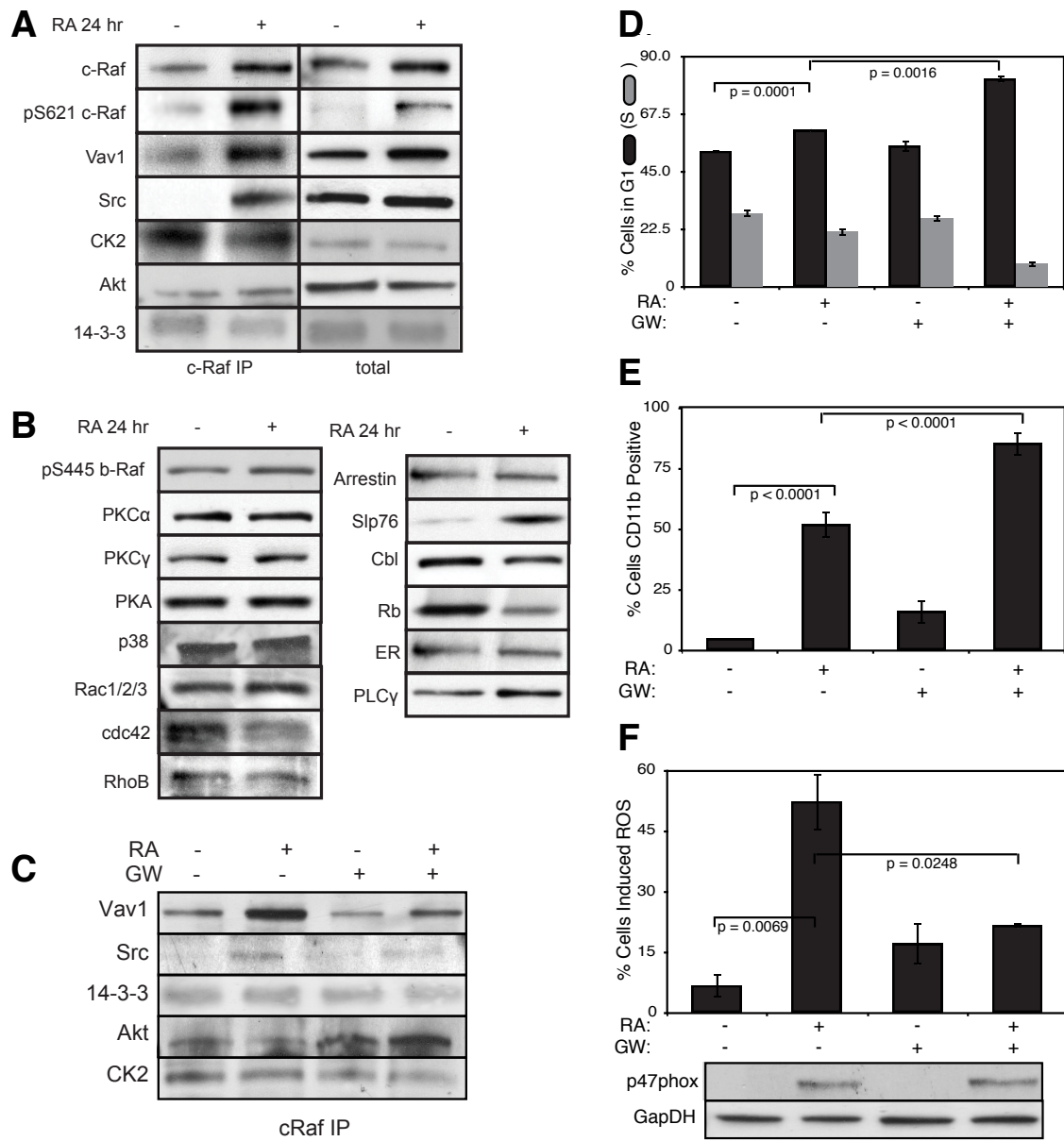


**Fig. 5:** Investigation of a panel of possible Raf interaction partners in the presence and absence of ATRA. A: Species identified to precipitate out with Raf: first column shows Western blot analysis on total Raf immunoprecipitation with and without 24 hr ATRA treatment and the second on total lysate. B: The expression of species considered that did not precipitate out with Raf at levels detectable by Western blot analysis on total lysate. C: Effect of the Raf inhibitor GW5074 on Raf interactions as determined by Western blot analysis of total Raf immunoprecipitation. The Authors note the signal associated with Src was found to be weak. D: Cell Cycle distribution as determined by flow cytometry indicated arrest induced by ATRA, which was increased by the addition of GW5074. E: Expression of the cell surface marker CD11b as determined by flow cytometry indicated increased expression induced by ATRA, which was enhanced by the addition of GW5074. F: Inducible reactive oxygen species (ROS) as determined by DCF flow cytometry. The functional differentiation response of ATRA treated cells was mitigated by GW5074.